Geophysical Research Letters

RESEARCH LETTER
10.1029/2024GL112756

The Sea Surface Temperature Pattern Effect on Outgoing Longwave Radiation: The Role of Large-Scale Convective Aggregation

Heng Quan[1,2], **Bosong Zhang**[2], **Chenggong Wang**[1,2], **and Stephan Fueglistaler**[1,2]

[1]Department of Geosciences, Princeton University, Princeton, NJ, USA, [2]Program in Atmospheric and Oceanic Sciences, Princeton University, Princeton, NJ, USA

Key Points:

- Tropical large-scale sea surface temperature (SST) gradients affect outgoing longwave radiation (OLR) by modulating the strength of large-scale convective aggregation
- The impact of SST gradients on OLR is comparable to that on shortwave cloud radiative effect, both with large inter-model spread
- Large-scale convective aggregation inferred from SST observations reduced global warming for the 1980–2010

Supporting Information:

Supporting Information may be found in the online version of this article.

Correspondence to:

H. Quan,
hengquan@princeton.edu

Citation:

Quan, H., Zhang, B., Wang, C., & Fueglistaler, S. (2025). The sea surface temperature pattern effect on outgoing longwave radiation: The role of large-scale convective aggregation. *Geophysical Research Letters*, *52*, e2024GL112756. https://doi.org/10.1029/2024GL112756

Received 25 SEP 2024
Accepted 25 APR 2025

Author Contributions:

Conceptualization: Heng Quan, Bosong Zhang, Stephan Fueglistaler
Formal analysis: Heng Quan
Methodology: Heng Quan, Chenggong Wang
Project administration: Stephan Fueglistaler
Supervision: Stephan Fueglistaler
Writing – original draft: Heng Quan
Writing – review & editing: Heng Quan, Bosong Zhang, Chenggong Wang, Stephan Fueglistaler

Abstract Observations and climate models show a strong increase/decrease of tropical low clouds, and hence reflected solar radiation, in response to an increase/decrease of the west-east sea surface temperature (SST) gradient in the tropical Pacific due to its impact on boundary layer inversion strength. Here, we discuss an accompanied increase/decrease of outgoing longwave radiation due to the contraction/expansion of the tropical deep convection area (decreasing/increasing the high cloud amount and relative humidity) when the SST gradient between regions with high and low SST increases/decreases. In targeted amip-piForcing style GFDL-AM4 model simulations, the negative longwave radiation response due to large-scale convective aggregation resulting from the La-Nina-like warming pattern over the period 1980–2010 is comparable to the negative shortwave cloud feedback. CMIP6 models show that the multi-model-mean is similar to that in our simulations. However, the relative magnitude of shortwave and longwave effects differs substantially between models, revealing an underappreciated climate model uncertainty.

Plain Language Summary The energy exchange between the Earth and the space is not only determined by the global mean surface temperature, but is also affected by its spatial pattern, especially the pattern of tropical Sea Surface Temperature (SST). Previous studies found that a larger west-east SST difference in the tropical Pacific generates more low-level clouds that reflect more solar radiation. Here, we demonstrate that a larger tropical SST difference also increases the energy emission from the Earth. This is because a larger SST difference narrows the area with strong ascending air, abundant water vapor, and high-level clouds, while expands the drier and clearer area. Consequently, the atmosphere (on average) becomes more transparent, resulting in more energy escaping to space. Thus, the SST change from 1980 to 2010 with increasing west-east SST difference in the tropical Pacific causes larger increase in both reflected solar radiation and energy emission from the Earth compared to a uniform warming case. They are of similar magnitude when averaged over different climate models, but individual models may have substantially different ratios between them, pointing to an underappreciated climate model uncertainty.

1. Introduction

The responses of the climate system to global warming are commonly normalized by the change in global mean surface temperature. The climate feedback parameter $(\lambda, [\mathrm{Wm^{-2}K^{-1}}])$ (the inverse of which sets the "climate sensitivity" given a fixed radiative forcing) is defined as the change of the top of atmosphere (TOA) net radiation per Kelvin global mean surface warming. However, recent studies have shown that in particular the geographical sea surface temperature (SST) warming pattern in the tropical Pacific strongly modulates the TOA net radiation response (Ceppi & Fueglistaler, 2021; Dong et al., 2019; Fueglistaler, 2019; Fueglistaler & Silvers, 2021; Gregory & Andrews, 2016; Stevens et al., 2016; Williams et al., 2023; B. Zhang et al., 2023; Zhou et al., 2017).

Generally, the focus of these analyses has been the impact of patterned SST trends on the average shortwave cloud radiative effect, which we summarize in Figure 1: Due to the weak temperature gradient in free-troposphere close to equator (Charney, 1963; Quan et al., 2025; Sobel et al., 2001) and the fact that deep convection at high SSTs (i.e., in the Pacific the Maritime continent warm pool) couples the free-tropospheric temperature to the surface temperature in these regions (Arakawa & Schubert, 1974; Emanuel et al., 1994), variations in the west-east SST gradient (a larger gradient in Figure 1b than in Figure 1a) in the tropical Pacific directly lead to variations in the average boundary layer inversion strength. The latter, in turn, strongly affects low cloud occurrence (Klein & Hartmann, 1993; Wood & Bretherton, 2006) and hence the global shortwave cloud radiative effect. Note that the

10.1029/2024GL112756

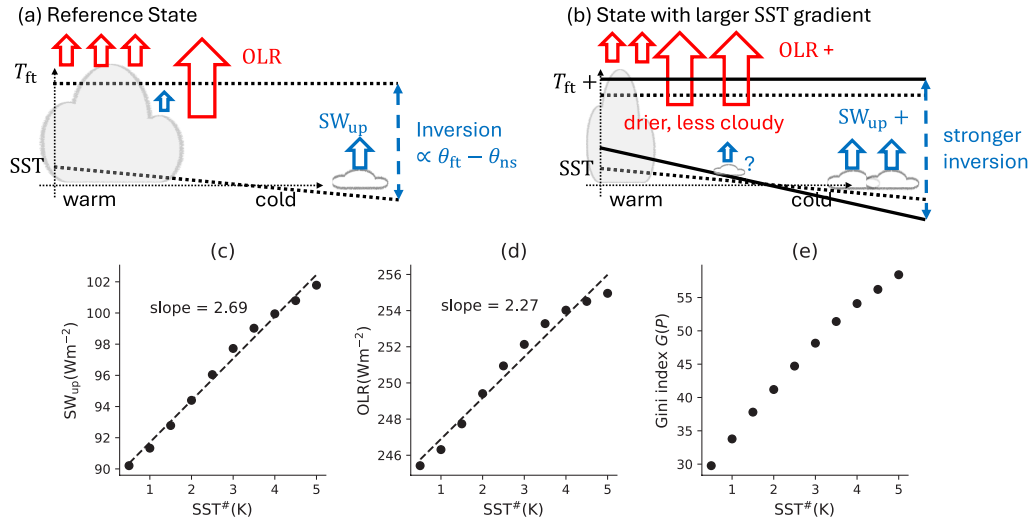

Figure 1. (a) Schematic of the impact of the tropical large-scale sea surface temperature (SST) gradient on cloud shortwave radiative effect and outgoing longwave radiation (OLR). The tropical free tropospheric temperature (T_{ft}) is set by the SST at the warm end of the domain where deep convection couples the boundary layer to the free troposphere. (b) A steepening of the SST gradient (generally: increase in SST difference between warm and cold regions) results in an increase in the boundary layer inversion strength (approximately proportional to the difference between free-tropospheric potential temperature and near-surface potential temperature, $\theta_{ft} - \theta_{ns}$) over the cold part of the domain, leading to more low clouds and more reflected shortwave radiation (blue arrows). A larger SST gradient also results in the large-scale aggregation of tropical deep convection due a higher (relative to the mean) convective threshold (Chou & Neelin, 2004; Neelin et al., 2003; Y. Zhang & Fueglistaler, 2019) and stronger up-gradient boundary layer moisture transport (Quan et al., 2024). This large-scale convective aggregation reduces the average free-tropospheric relative humidity and high cloud amount, resulting in an increase in OLR (red arrows) (Becker & Wing, 2020; Bony et al., 2020; McKim et al., 2021; Schiro et al., 2022; B. Zhang et al., 2021); the effect on shortwave reflection in the deep convective region is less certain (indicated with question mark; not discussed in this paper) due to possible compensation between high and low cloud changes. (c–e) The tropical (30°S to 30°N) mean top of atmosphere upward shortwave radiation (SW_{up}), mean OLR and the degree of large-scale convective aggregation quantified with the Gini index of the tropical precipitation distribution $G(P)$ as a function of SST (a metric for the SST gradient, see methods). Results show idealized simulations (see text) with AM4 developed by NOAA/Geophysical Fluid Dynamics Laboratory.

effect is not restricted to the tropical Pacific, but the discussion in terms of "SST gradient" is simpler and may be more intuitive than the general characterization in terms of SST variance, SST interquartile range, or SST difference between warm and cold regions.

In the following, we show that in Atmospheric General Circulation Model (GCM) simulations, the impact of the large-scale tropical SST gradient on OLR through its control on the large-scale aggregation of deep convection (Figures 1a and 1b) is comparable to its impact on the shortwave cloud radiative effect. Further, it is shown that in these models the shortwave and longwave effects are generally positively correlated as may be expected from basic reasoning as sketched in Figures 1a and 1b. That is, in most models the longwave effect has the same sign as the shortwave effect on the top-of-atmosphere radiative balance, but the relative magnitudes may differ substantially between different models.

The paper is organized as follows. Section 2 describes the numerical simulations and the metric for measuring large-scale convective aggregation used in this study. Section 3 presents the main results: (a) Idealized SST gradient perturbation simulations demonstrate that the tropical SST gradient affects OLR primarily by modulating the strength of large-scale convective aggregation and (b) targeted atmospheric GCM simulations with prescribed sea surface temperatures and fixed pre-industrial forcings (similar to the CMIP6 amip piControl experiment) show that the large-scale convective aggregation over the period 1980–2010 due to the La-Nina-like SST warming pattern is the main cause of the enhanced OLR increase relative to a uniform SST warming pattern. In these simulations, the longwave effect is comparable to the enhanced shortwave cloud radiative effect, and contributes to a more negative (stabilizing) climate feedback for the period 1980–2010 than that expected based on coupled atmosphere-ocean GCMs for long-term CO_2 increase. Finally, Section 4 summarizes the results and conclusions, and discusses implications.

2. Methods

2.1. General Circulation Model (GCM) Simulations

We use the Geophysical Fluid Dynamics Laboratory atmospheric GCM AM4 (Zhao et al., 2018a, 2018b) to conduct SST perturbation simulations. AM4 uses a horizontal grid spacing of approximately 100 km and saves the data to disk on a grid with 180 grid points in the meridional, and 288 grid point in the zonal direction (i.e., $1.0^\circ \times 1.25^\circ$ for the horizontal resolution). The SST perturbations (defined below) are applied to a control simulation forced by the observed climatological (1982–2001) monthly means of SSTs and sea ice concentrations from the HADISST1 data set (Rayner et al., 2003). The greenhouse gas concentrations and aerosol emissions correspond to the conditions of the year 2000 and are not modified in the perturbation simulations. The control simulation and the perturbation simulations are integrated for 45 years, with the first 5 years discarded to eliminate spin-up effects. All results below show averaged fields computed from the monthly mean fields of the last 40 years of the model simulations.

The following perturbations are applied to the control state SSTs:

1. Idealized tropical SST gradient perturbation simulations. Following Fueglistaler (2019), we quantify the tropical (between 30°S to 30°N) SST gradient by SST, defined as the average temperature of the warmest 30% minus the tropical average SST. For any target $\mathrm{SST}^{\#}_{\mathrm{target}}$, the tropical SST field (between 30°S to 30°N) in the perturbation simulation is given by

$$\mathrm{SST} = \overline{\mathrm{SST}}_{\mathrm{control}} + \frac{\mathrm{SST}^{\#}_{\mathrm{target}}}{\mathrm{SST}^{\#}_{\mathrm{control}}} \times \left(\mathrm{SST}_{\mathrm{control}} - \overline{\mathrm{SST}}_{\mathrm{control}}\right), \tag{1}$$

   where "control" denotes the control simulation and the overbar symbol stands for the average over the tropics. SSTs outside the tropics are not perturbed. The SST perturbation as specified in Equation 1 perturbs the magnitude of the range of tropical SSTs without changing the tropical average SST. The control simulation has SST = 2.45 K, and we run 10 perturbation simulations covering the range from SST = 0.5 to SST = 5.0 K (with an increment of 0.5 K).
2. A simulation using the SST trend pattern of the period 1980 to 2010, where the local SST perturbation equals to the linear trend (at each grid cell) of the HADISST1 SST data (Rayner et al., 2003) from 1980 to 2010; the experiment applies the effective change over the 30 years as given by the linear regression to exclude the effect of internal variability.
3. A uniform SST +4 K simulation for comparison with the patterned warming simulation.

2.2. The Gini Index: A Metric for Large-Scale Convective Aggregation

Following Y. Zhang and Fueglistaler (2019), we use the Gini index, an index for inequality frequently used in economics to quantify the unevenness of income and wealth, of tropical (between 30°S and 30°N) precipitation as a metric for the spatial aggregation of tropical deep convection (Pendergrass & Knutti, 2018). The calculation of the Gini index is illustrated in Quan et al. (2024) (their Figure 2a). The Gini index $G(P)$ ranges from 0 (completely uniform deep convection) to 100 (all deep convection is located in one model grid cell), and an increase in the Gini index indicates a stronger spatial aggregation of deep convection (narrower convective regions). Another metric of large-scale aggregation—the tropical ascent fraction (Bony et al., 2006; Su et al., 2017)—is well correlated with the Gini index (the correlation coefficient is −0.84) in these idealized simulations (see Figure S1 in Supporting Information S1).

3. Results

3.1. The Role of Large-Scale Convective Aggregation

We first show the results of the idealized AM4 SST gradient perturbation simulations (Section 2). Figures 1c and 1d shows that both tropical mean OLR and reflected (upward) shortwave radiation ($\mathrm{SW_{up}}$) increase with increasing tropical SST gradient (measured by SST) in the idealized AM4 simulations, with a similar sensitivity to the SST gradient perturbation and strong correlation (the correlation coefficient between $\mathrm{SW_{up}}$ and OLR is 0.997). Figure 2 decomposes the results of these simulations over the tropical ocean into SST percentiles. In

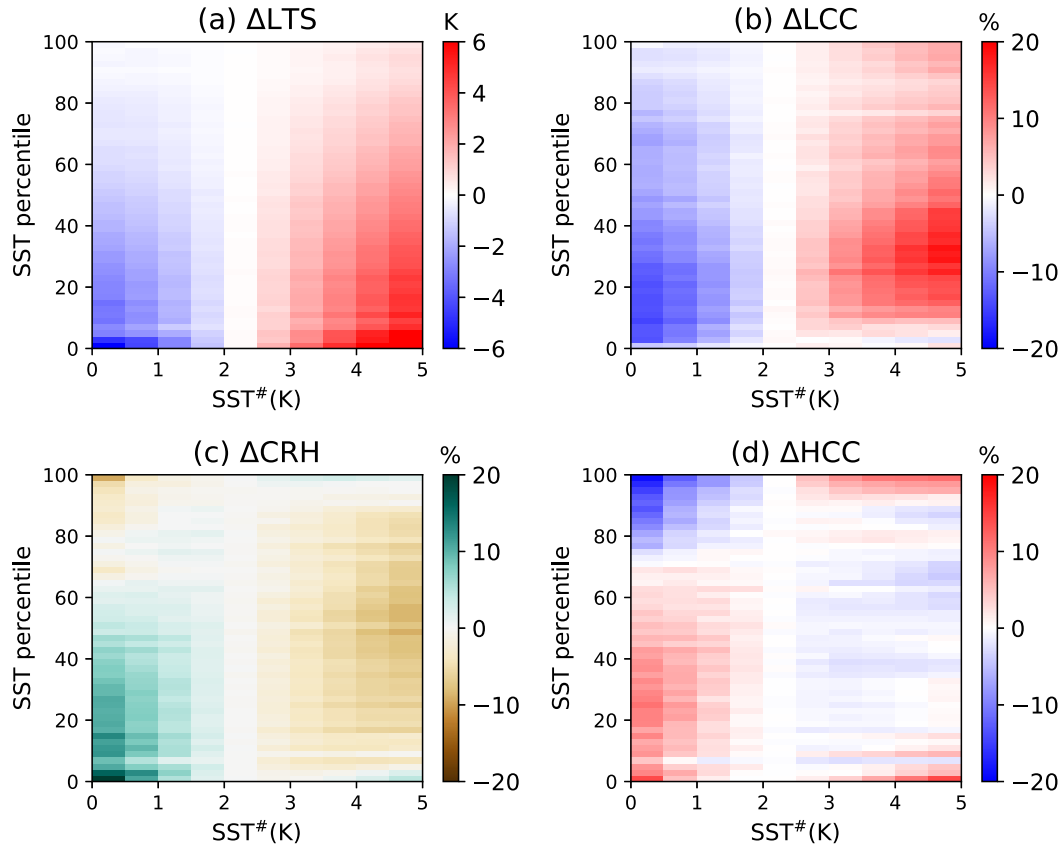

Figure 2. Responses (perturbation run minus control run) of tropical (30°S to 30°N) mean (a) static stability of lower troposphere (the difference between 700 hPa potential temperature and sea level potential temperature), (b) low cloud cover, (c) column relative humidity (water vapor mass divided by saturated water vapor mass between 850 and 200 hPa), and (d) high cloud cover for idealized AM4 simulations with different SST (*x*-axis), binned into sea surface temperature percentiles (*y*-axis), with sorting from cold (percentile 1) to warm (percentile 100).

general (Figures 1a and 1b), deep convection occurs at the warm end (high percentile). Figure 2 shows that the domain-mean correlations shown in Figures 1c and 1d indeed result from the mechanism as sketched in Figures 1a and 1b. Figure 2a shows that an increase/decrease of the cold-warm contrast (SST) increases/decreases the boundary layer inversion strength over the colder ocean, but has little impact on the boundary layer inversion strength over the warm ocean. Correspondingly, the low cloud amount (Figure 2b) increases/decreases over the cold ocean as expected, reflecting more/less solar radiation. Note that, as indicated in the sketch (Figures 1a and 1b), the degree of compensation between a decrease in high cloud amount and an increase in low cloud amount upon contraction of the convective domain also affects reflected shortwave radiation, but may depend on the cloud parametrization scheme and differ between models.

The increase in OLR with increasing SST but fixed average SST (Figure 1d) is the focus of this paper. At fixed relative humidity, the clear-sky OLR is approximately linearly related to the (average) surface temperature (Koll & Cronin, 2018; McKim et al., 2021; Y. Zhang et al., 2020), which cannot explain the approximately linear relation between OLR and SST in these model simulations with fixed average SST. Thus, Figure 1d highlights the impact of large-scale convective aggregation on OLR. As the SST gradient becomes larger, the resultant warming of the tropical free-troposphere raises the threshold (relative to the mean SST) of deep convection. The tropical free-tropospheric moist static energy (MSE) increase is approximately spatially uniform (Charney, 1963; Quan et al., 2025; Sobel et al., 2001) and set by the near-surface MSE increase over the warmest SSTs through deep convection (Arakawa & Schubert, 1974; Emanuel et al., 1994; Y. Zhang & Fueglistaler, 2020). Marginal regions where the subcloud MSE increases less than in the region of highest SSTs are no longer convective (Neelin et al., 2003; Y. Zhang & Fueglistaler, 2019). A larger SST gradient also causes a stronger boundary layer

circulation (Lindzen & Nigam, 1987), which increases the up-gradient moisture transport from subsiding regions to convective regions (Quan et al., 2024).

These two effects together cause stronger convection over the warmest SSTs and weaker convection elsewhere, which means a stronger large-scale convective aggregation (represented by a larger Gini index of tropical precipitation in Figure 1e) associated with the expansion of dry and clear-sky regions. As shown by Figures 2c and 2d, a larger (smaller) SST gradient (i.e., stronger convective aggregation) causes the decrease (increase) of column relative humidity (CRH) and high cloud amount at the intermediate SST percentiles, which increases (decreases) the tropical average OLR. At the highest SST percentiles, a larger SST gradient strengthens local deep convection, which increases column RH and high cloud amount. The responses at the intermediate SST percentiles are dominant and consistent with the relation between convective organization and OLR reported in previous studies (Becker & Wing, 2020; Bony et al., 2020; Schiro et al., 2022), confirming the schematic in Figures 1a and 1b. Note, however, that the aggregation of interest here occurs on the planetary scale, rather than in previously reported small-domain cloud resolving simulations without external forcing (e.g., Muller & Held, 2012; Wing et al., 2018). Finally, we note that the responses at the very lowest SST percentiles do not follow the pattern and may reflect changes at the edges of the tropics where the changes are not controlled by tropical dynamics anymore.

The large-scale convective aggregation seen in the GCM simulations (Figure 2) may be affected by parameterizations in particular of the convective processes. To test the robustness of our theory, we perform additional cloud-resolving model (CRM) mock-Walker simulations (Text S1 in Supporting Information S1) that rely on fewer parameterizations and explicity resolve deep convection. We find that the CRM mock-Walker simulations show (Figures S2 and S3 in Supporting Information S1) the same effect as the GCM simulations, adding confidence that the GCM results are physically robust and not unduly affected by parameterizations and uncertainties therein.

Because in global warming experiments with coupled atmosphere-ocean GCMs (CMIP5 RCP8.5) the warmest waters with atmospheric deep convection only warm about 10% more than the tropical average SST (Fueglistaler & Silvers, 2021), neither the shortwave nor the longwave radiation responses in these simulations show a strong signature of departure from the responses to uniform SST warming (Schiro et al., 2022). However, the situation is very different for the historical period. In particular, between the late 1970s and early 2000s, the amplification of the tropical SST gradient is about 50% (Fueglistaler & Silvers, 2021), which induces a strong negative feedback (Armour et al., 2024; Fueglistaler & Silvers, 2021).

3.2. The Effect of the 1980–2010 SST Trend Pattern on OLR

In the following, we quantify the contribution of large-scale convective aggregation to the negative longwave feedback over the period 1980–2010. In order to isolate the effect of the observed SST trend over this period on OLR, we analyze targeted amip-piForcing style simulations with all forcing agents except SST fixed. We compare the radiative flux responses (normalized by tropical average surface temperature change) of the AM4 atmospheric GCM with prescribed uniform +4 K SST increase to the simulation with the patterned historical SST change over the period 1980–2010 (see Section 2).

The historical pattern effect (i.e., the difference "historical patterned warming" simulation minus "uniform warming" simulation) results (Table S1 in Supporting Information S1) are consistent with the expectations as shown in the schematic (Figure 1): Compared with the uniform +4 K simulation, the response of the historical simulation with a La-Nina-like SST warming pattern shows a larger increase in reflected shortwave radiation of $\Delta \frac{\mathrm{dSW_{up}}}{\mathrm{d}\overline{T_s}} = 1.93 \mathrm{Wm^{-2}K^{-1}}$ and a larger increase of OLR of $\Delta \frac{\mathrm{dOLR}}{\mathrm{d}\overline{T_s}} = 1.45 \mathrm{Wm^{-2}K^{-1}}$. We also calculate the change in lower tropospheric stability, low cloud cover, CRH, high cloud cover, $\mathrm{SST^{\#}}$, and the Gini index $G(P)$ of tropical precipitation; and their differences between the two experiments. We find that the larger $\mathrm{SW_{up}}$ increase is due to an enhanced increase in lower troposphere stability and low cloud amount, while the larger OLR increase is due to enhanced free-tropospheric warming, free-tropospheric drying and high cloud reduction as a result of a much stronger convective aggregation. Note that the sign of the changes provides support to the physical reasoning (Figure 1), and the numerical simulations reveal that the magnitude of the shortwave and longwave effect are very similar for this atmospheric GCM.

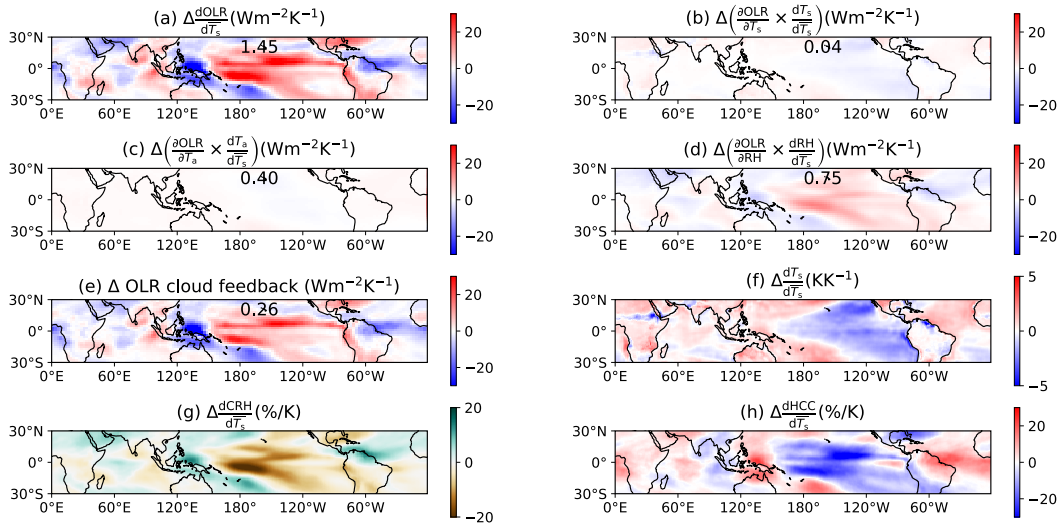

Figure 3. (a) The difference of tropical (30°S to 30°N) average outgoing longwave radiation responses $\frac{\mathrm{dOLR}}{\mathrm{d}\overline{T_s}}$ (normalized to +1 K tropical mean surface warming) between the AM4 historical sea surface temperature (SST) perturbation simulation and the uniform SST +4 K simulation (historical minus uniform +4 K), decomposed into contributions from (b) surface temperature, (c) atmospheric temperature, (d) atmospheric relative humidity, and (e) could field using the radiative kernel (Equation 2), and with the tropical mean values marked in each plot. (f–h) Similar to (a) but for surface temperature (T_s), column relative humidity and high cloud cover.

Additional simulations with a uniform +1 K warming rather than +4 K show a weak non-linearity. The effect of the patterned warming evaluated against the +1 K simulations shows a slightly larger shortwave effect $\left(\Delta\frac{\mathrm{dSW_{up}}}{\mathrm{d}\overline{T_s}}=2.20\mathrm{Wm^{-2}K^{-1}}\right)$, and a slightly smaller longwave effect $\left(\Delta\frac{\mathrm{dOLR}}{\mathrm{d}\overline{T_s}}=1.36\mathrm{Wm^{-2}K^{-1}}\right)$; see also Table S2 in Supporting Information S1.

The sign of the OLR trend difference between patterned and uniform warming is as expected considering the large-scale aggregation mechanism. However, further analysis is needed to provide proof that the cause is indeed large scale aggregation and not other processes (e.g., free-tropospheric warming only). In order to quantify the contribution of the large-scale convective aggregation to the longwave feedback difference, we use the radiative kernel approach (Soden et al., 2008) to decompose the OLR budget at each model grid cell into a contribution from: local surface temperature (T_s), atmospheric temperature (T_a), atmospheric relative humidity (RH), and cloud field.

$$\frac{\mathrm{dOLR}}{\mathrm{d}\overline{T_s}}=\frac{\partial \mathrm{OLR}}{\partial T_s}\frac{\mathrm{d}T_s}{\mathrm{d}\overline{T_s}}+\frac{\partial \mathrm{OLR}}{\partial T_a}\frac{\mathrm{d}T_a}{\mathrm{d}\overline{T_s}}+\frac{\partial \mathrm{OLR}}{\partial \mathrm{RH}}\frac{\mathrm{dRH}}{\mathrm{d}\overline{T_s}}+\text{OLR cloud feedback.} \quad (2)$$

Note that we use surface temperature, atmospheric temperature, and relative humidity rather than absolute humidity since the "lapse rate feedback" and the "specific humidity" feedback approximately cancel (Held & Shell, 2012; Jeevanjee et al., 2021). The OLR cloud feedback is computed as the residual, which is a fair estimation because we are interested in the *differences* between the two simulations (i.e., the biases in the kernel offline estimate compared to the GCM calculation can be expected to approximately cancel).

Figure 3 shows the maps of the *differences* between the two simulations of the decomposition terms in Equation 2. The figure shows that the historical SST pattern effect on OLR is dominated by the RH contribution $\frac{\partial \mathrm{OLR}}{\partial \mathrm{RH}}\frac{\mathrm{dRH}}{\mathrm{d}\overline{T_s}}$ and the cloud feedback. They both show a decrease in OLR in the western Pacific warm pool and an increase in OLR in adjacent regions, consistent with a contraction (aggregation) of the region of deep convection. The RH contribution and the cloud feedback together account for 70% of tropical mean $\frac{\mathrm{dOLR}}{\mathrm{d}\overline{T_s}}$ ($1.01\mathrm{Wm^{-2}K^{-1}}$ in $1.45\mathrm{Wm^{-2}K^{-1}}$), and they are indeed explained by large-scale convective aggregation: The post 1980 La-Nina-like SST warming pattern (Figure 3f) narrows the convective area in the western Pacific warm pool, associated with enhanced free-tropospheric drying (Figure 3g) and high cloud reduction (Figure 3h) in adjacent regions

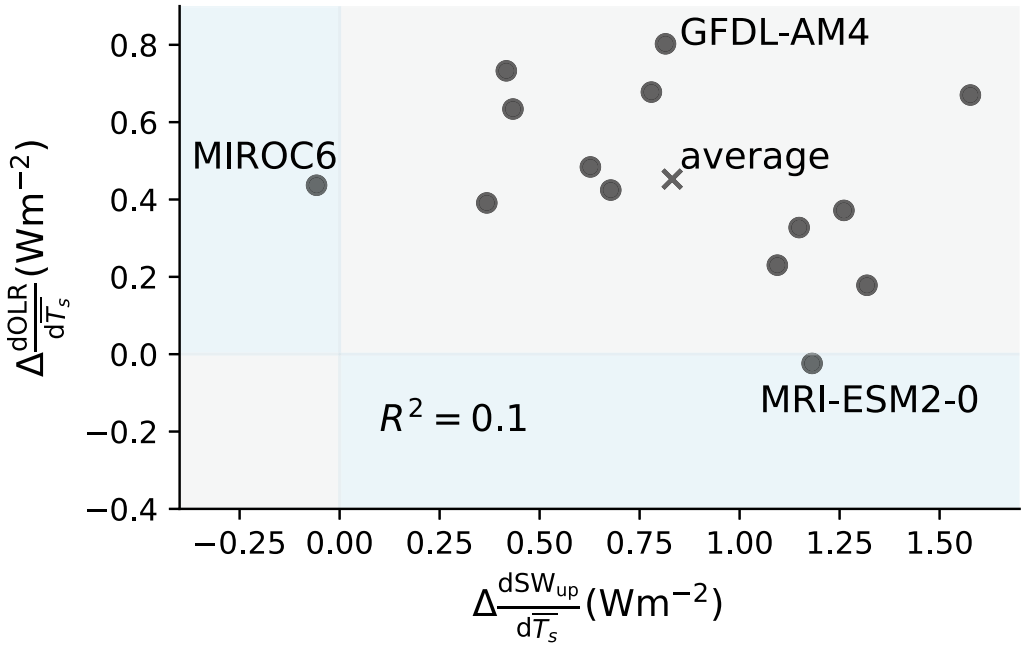

Figure 4. The difference of the global mean $\frac{\mathrm{dSW_{up}}}{\mathrm{d}\overline{T_s}}$ (x-axis) and $\frac{\mathrm{dOLR}}{\mathrm{d}\overline{T_s}}$ (y-axis) between the CMIP6 amip-piForcing simulations (1980–2010) and the abrupt 4xCO_2 simulations (150 years) for different CMIP6 models. Detailed results for individual models are listed in Table S3 in Supporting Information S1. The original data is from Andrews et al. (2022).

(especially the central Pacific). A similar effect (but with smaller amplitude) is also visible over the central Indian ocean. Previous studies (Andrews & Webb, 2018; Andrews et al., 2022) attributed the enhanced (relative to uniform warming) OLR increase primarily to enhanced free tropospheric warming, whereas our analysis indicates that the enhanced OLR is primarily due to large-scale convective aggregation.

In order to evaluate the inter-model spread of the radiative effect due to large-scale convective aggregation, we turn to the CMIP6 data archive and compare the amip-piForcing simulations (1980–2010) with the abrupt 4xCO_2 simulations (150 years). The 4xCO_2 simulations show a much more uniform SST warming pattern than the historical amip-piForcing simulations. The difference between these two experiments is the best approximation to evaluate the effect with the experiments stored in the CMIP6 archive, and allows direct comparison with Andrews et al. (2022) that focused on cloud radiative effects.

For both experiments, we calculate the global mean $\frac{\mathrm{dSW_{up}}}{\mathrm{d}\overline{T_s}}$, $\frac{\mathrm{dOLR}}{\mathrm{d}\overline{T_s}}$, and $\frac{\mathrm{dOLR_{cs}}}{\mathrm{d}\overline{T_s}}$ (clear-sky OLR), using the data provided by Andrews et al. (2022); our analysis complements their analysis of the data in terms of differences in cloud radiative effects versus clear sky radiative fluxes. Figure 4 shows that most models have both enhanced OLR and enhanced reflection of shortwave radiation in the historical simulations (La-Nina like warming pattern) compared to the 4xCO_2 simulations (fairly uniform warming pattern), following the expectation (Figure 1) that the two effects should have the same sign. On average, the enhanced $\mathrm{SW_{up}}$ increase contributes about 65% $\left(0.83\mathrm{Wm}^{-2}\mathrm{K}^{-1}\right)$ to the TOA net radiation trend difference, and the enhanced OLR increase contributes about 35% $\left(0.45\mathrm{Wm}^{-2}\mathrm{K}^{-1}\right)$. Thus, in the multi-model mean, the two effects are of comparable magnitude.

The inter-model spread of the 1980–2010 enhanced clear-sky OLR increase is small (ranging from $0.4\mathrm{Wm}^{-2}\mathrm{K}^{-1}$ to $0.5\mathrm{Wm}^{-2}\mathrm{K}^{-1}$ for most models in Table S3 in Supporting Information S1), indicating that the large-scale aggregation and associated atmospheric drying are robust among models. Conversely, the longwave cloud radiative effect trend differences between models are large. Alessi and Rugenstein (2023) show in their Figure S4 in Supporting Information S1 that a larger tropical SST gradient results in a positive longwave cloud radiative effect (i.e., the response of clouds reduces OLR) in the MPI-ESM model, whereas we find (Table S3 in Supporting Information S1) that other models (including GFDL-AM4 used here) yield a negative longwave cloud radiative effect (consistent with Figures 1a and 1b). Also, the intermodel range of the relative magnitude of the (all

sky) longwave versus shortwave effect is large. Figure 4 shows that the MIROC6 model attributes almost all of the total effect to the longwave convective aggregation effect, GFDL-AM4 attributes about half to long- and shortwave each, and the MRI-ESM2-0 model attributes almost all to the shortwave effect. One may speculate that the physically plausible coupling between the shortwave and longwave radiative effect may lead to a correlation between the two across models. However, this is not so $\left(r^2 \approx 0.1\right)$, pointing to a need to further investigate why different models show such a large spread in the relative contributions from shortwave and longwave radiation.

4. Conclusions and Discussions

The spatial pattern of tropical SST affects TOA radiation and climate sensitivity. The analysis presented here focuses on longwave radiation, complementing previous studies that focused on the shortwave cloud radiative effect (Ceppi & Fueglistaler, 2021; Dong et al., 2019; Fueglistaler, 2019; Fueglistaler & Silvers, 2021; Gregory & Andrews, 2016; Williams et al., 2023; Zhou et al., 2017). Our analysis shows that the tropical SST gradient affects OLR by modulating the strength of large-scale convective aggregation (Figures 1 and 2): A larger SST gradient narrows the convective area, associated with the expansion of dry and clear-sky regions, both leading to an increase in OLR.

Further, we show that the large-scale convective aggregation over the period 1980–2010 contributes to the enhanced OLR increase in the amip-piForcing style simulation (Figure 3) compared to a uniform SST warming case. The La-Nina-like SST warming pattern post 1980 narrows the convective area in the western Pacific warm pool compared to uniform warming, leading to free-tropospheric drying and high cloud reduction in adjacent regions (especially the central Pacific).

The enhanced (relative to a geographically uniform warming of the ocean surface) OLR increase over the period 1980–2010 in the amip-piForcing style simulation is comparable to the enhanced reflected shortwave radiation in the targeted AM4 simulations (Table S1 in Supporting Information S1). Analysis of CMIP6 experiments shows that on average, the models have a comparable magnitude of the longwave and shortwave effect, but the inter-model spread of the partitioning is large (Figure 4). The notion of a warming-pattern induced anomalously negative radiative feedback from 1980 to 2010 is consistent with previous results (Armour et al., 2024; Fueglistaler & Silvers, 2021; Zhou et al., 2016). However, the large inter-model spread of net, and partitioning between long- and short-wave effect, reported here indicates a substantially larger uncertainty between models than indicated by the results of Schiro et al. (2022) who analyzed the role of large-scale convective aggregation for inter-model differences in climate sensitivity. A plausible explanation for the differing conclusions is that the coupled atmosphere-ocean GCMs global warming simulations analyzed by Schiro et al. (2022) show only a small magnitude of the SST pattern change relative to the mean warming (Fueglistaler & Silvers, 2021), and hence the effect from aggregation is small compared to that of other processes. Our results reinforce the importance of large-scale convective aggregation on the radiative feedback and climate sensitivity, and highlight the need to improve understanding of the differences therein between atmospheric GCMs.

Data Availability Statement

The data derived from CMIP6 data can be found at https://doi.org/10.5281/zenodo.6799004 (Andrews et al., 2022). The radiative kernel analysis follows methods provided by Chenggong Wang at https://github.com/ChenggongWang/Radiative_Response_with_Radiative_Kernel.

Acknowledgments
Heng Quan thanks Jing Feng, Gabriel Vecchi, and Paulo Ceppi for helpful discussions. We thank Marat F. Khairoutdinov for creating and maintaining SAM. We thank two anonymous reviewers for their helpful review comments. This report was prepared by Heng Quan under Award A18OAR4320123 from the National Oceanic and Atmospheric Administration, U.S. Department of Commerce. The statements, findings, conclusions, and recommendations are those of the author(s) and do not necessarily reflect the views of the National Oceanic and Atmospheric Administration, or the U.S. Department of Commerce.

References

Alessi, M. J., & Rugenstein, M. A. (2023). Surface temperature pattern scenarios suggest higher warming rates than current projections. *Geophysical Research Letters*, *50*(23), e2023GL105795. https://doi.org/10.1029/2023gl105795

Andrews, T., Bodas-Salcedo, A., Gregory, J. M., Dong, Y., Armour, K. C., Paynter, D., et al. (2022). On the effect of historical SST patterns on radiative feedback. *Journal of Geophysical Research: Atmospheres*, *127*(18), e2022JD036675. https://doi.org/10.1029/2022jd036675

Andrews, T., & Webb, M. J. (2018). The dependence of global cloud and lapse rate feedbacks on the spatial structure of tropical Pacific warming. *Journal of Climate*, *31*(2), 641–654. https://doi.org/10.1175/jcli-d-17-0087.1

Arakawa, A., & Schubert, W. H. (1974). Interaction of a cumulus cloud ensemble with the large-scale environment, part I. *Journal of the Atmospheric Sciences*, *31*(3), 674–701. https://doi.org/10.1175/1520-0469(1974)031<0674:ioacce>2.0.co;2

Armour, K. C., Proistosescu, C., Dong, Y., Hahn, L. C., Blanchard-Wrigglesworth, E., Pauling, A. G., et al. (2024). Sea-surface temperature pattern effects have slowed global warming and biased warming-based constraints on climate sensitivity. *Proceedings of the National Academy of Sciences of the United States of America*, *121*(12), e2312093121. https://doi.org/10.1073/pnas.2312093121

Becker, T., & Wing, A. A. (2020). Understanding the extreme spread in climate sensitivity within the radiative-convective equilibrium model intercomparison project. *Journal of Advances in Modeling Earth Systems*, *12*(10), e2020MS002165. https://doi.org/10.1029/2020ms002165

Bony, S., Colman, R., Kattsov, V. M., Allan, R. P., Bretherton, C. S., Dufresne, J.-L., et al. (2006). How well do we understand and evaluate climate change feedback processes? *Journal of Climate*, *19*(15), 3445–3482. https://doi.org/10.1175/jcli3819.1

Bony, S., Semie, A., Kramer, R., Soden, B., Tompkins, A., & Emanuel, K. (2020). Observed modulation of the tropical radiation budget by deep convective organization and lower-tropospheric stability. *AGU Advances*, *1*(3), e2019AV000155. https://doi.org/10.1029/2019av000155

Ceppi, P., & Fueglistaler, S. (2021). The El Niño–Southern Oscillation pattern effect. *Geophysical Research Letters*, *48*(21), e2021GL095261. https://doi.org/10.1029/2021gl095261

Charney, J. G. (1963). A note on large-scale motions in the tropics. *Journal of the Atmospheric Sciences*, *20*(6), 607–609. https://doi.org/10.1175/1520-0469(1963)020<0607:anolsm>2.0.co;2

Chou, C., & Neelin, J. D. (2004). Mechanisms of global warming impacts on regional tropical precipitation. *Journal of Climate*, *17*(13), 2688–2701. https://doi.org/10.1175/1520-0442(2004)017<2688:mogwio>2.0.co;2

Dong, Y., Proistosescu, C., Armour, K. C., & Battisti, D. S. (2019). Attributing historical and future evolution of radiative feedbacks to regional warming patterns using a Green's function approach: The preeminence of the western Pacific. *Journal of Climate*, *32*(17), 5471–5491. https://doi.org/10.1175/jcli-d-18-0843.1

Emanuel, K. A., David Neelin, J., & Bretherton, C. S. (1994). On large-scale circulations in convecting atmospheres. *Quarterly Journal of the Royal Meteorological Society*, *120*(519), 1111–1143. https://doi.org/10.1002/qj.49712051902

Fueglistaler, S. (2019). Observational evidence for two modes of coupling between sea surface temperatures, tropospheric temperature profile, and shortwave cloud radiative effect in the tropics. *Geophysical Research Letters*, *46*(16), 9890–9898. https://doi.org/10.1029/2019gl083990

Fueglistaler, S., & Silvers, L. (2021). The peculiar trajectory of global warming. *Journal of Geophysical Research: Atmospheres*, *126*(4), e2020JD033629. https://doi.org/10.1029/2020jd033629

Gregory, J. M., & Andrews, T. (2016). Variation in climate sensitivity and feedback parameters during the historical period. *Geophysical Research Letters*, *43*(8), 3911–3920. https://doi.org/10.1002/2016gl068406

Held, I. M., & Shell, K. M. (2012). Using relative humidity as a state variable in climate feedback analysis. *Journal of Climate*, *25*(8), 2578–2582. https://doi.org/10.1175/jcli-d-11-00721.1

Jeevanjee, N., Koll, D. D., & Lutsko, N. (2021). "Simpson's Law" and the spectral cancellation of climate feedbacks. *Geophysical Research Letters*, *48*(14), e2021GL093699. https://doi.org/10.1029/2021gl093699

Klein, S. A., & Hartmann, D. L. (1993). The seasonal cycle of low stratiform clouds. *Journal of Climate*, *6*(8), 1587–1606. https://doi.org/10.1175/1520-0442(1993)006<1587:tscols>2.0.co;2

Koll, D. D., & Cronin, T. W. (2018). Earth's outgoing longwave radiation linear due to H_2O greenhouse effect. *Proceedings of the National Academy of Sciences of the United States of America*, *115*(41), 10293–10298. https://doi.org/10.1073/pnas.1809868115

Lindzen, R. S., & Nigam, S. (1987). On the role of sea surface temperature gradients in forcing low-level winds and convergence in the tropics. *Journal of the Atmospheric Sciences*, *44*(17), 2418–2436. https://doi.org/10.1175/1520-0469(1987)044<2418:otross>2.0.co;2

McKim, B. A., Jeevanjee, N., & Vallis, G. K. (2021). Joint dependence of longwave feedback on surface temperature and relative humidity. *Geophysical Research Letters*, *48*(18), e2021GL094074. https://doi.org/10.1029/2021gl094074

Muller, C. J., & Held, I. M. (2012). Detailed investigation of the self-aggregation of convection in cloud-resolving simulations. *Journal of the Atmospheric Sciences*, *69*(8), 2551–2565. https://doi.org/10.1175/jas-d-11-0257.1

Neelin, J., Chou, C., & Su, H. (2003). Tropical drought regions in global warming and El Niño teleconnections. *Geophysical Research Letters*, *30*(24), 2275. https://doi.org/10.1029/2003gl018625

Pendergrass, A. G., & Knutti, R. (2018). The uneven nature of daily precipitation and its change. *Geophysical Research Letters*, *45*(21), 11–980. https://doi.org/10.1029/2018gl080298

Quan, H., Zhang, B., Wang, C., & Fueglistaler, S. (2024). Non-linear radiative response to patterned global warming due to convection aggregation and non-linear tropical dynamics. *Journal of Climate*, *37*(21), 5675–5686. https://doi.org/10.1175/jcli-d-23-0539.1

Quan, H., Zhang, Y., & Fueglistaler, S. (2025). Weakening of tropical free-tropospheric temperature gradients with global warming. *Journal of the Atmospheric Sciences*, *82*(1), 31–43. https://doi.org/10.1175/jas-d-24-0140.1

Rayner, N., Parker, D. E., Horton, E., Folland, C. K., Alexander, L. V., Rowell, D., et al. (2003). Global analyses of sea surface temperature, sea ice, and night marine air temperature since the late nineteenth century. *Journal of Geophysical Research*, *108*(D14), 4407. https://doi.org/10.1029/2002jd002670

Schiro, K. A., Su, H., Ahmed, F., Dai, N., Singer, C. E., Gentine, P., et al. (2022). Model spread in tropical low cloud feedback tied to overturning circulation response to warming. *Nature Communications*, *13*(1), 7119. https://doi.org/10.1038/s41467-022-34787-4

Sobel, A. H., Nilsson, J., & Polvani, L. M. (2001). The weak temperature gradient approximation and balanced tropical moisture waves. *Journal of the Atmospheric Sciences*, *58*(23), 3650–3665. https://doi.org/10.1175/1520-0469(2001)058<3650:twtgaa>2.0.co;2

Soden, B. J., Held, I. M., Colman, R., Shell, K. M., Kiehl, J. T., & Shields, C. A. (2008). Quantifying climate feedbacks using radiative kernels. *Journal of Climate*, *21*(14), 3504–3520. https://doi.org/10.1175/2007jcli2110.1

Stevens, B., Sherwood, S. C., Bony, S., & Webb, M. J. (2016). Prospects for narrowing bounds on Earth's equilibrium climate sensitivity. *Earth's Future*, *4*(11), 512–522. https://doi.org/10.1002/2016ef000376

Su, H., Jiang, J. H., Neelin, J. D., Shen, T. J., Zhai, C., Yue, Q., et al. (2017). Tightening of tropical ascent and high clouds key to precipitation change in a warmer climate. *Nature Communications*, *8*(1), 1–9. https://doi.org/10.1038/ncomms15771

Williams, A. I., Jeevanjee, N., & Bloch-Johnson, J. (2023). Circus tents, convective thresholds, and the non-linear climate response to tropical SSTs. *Geophysical Research Letters*, *50*(6), e2022GL101499. https://doi.org/10.1029/2022gl101499

Wing, A. A., Emanuel, K., Holloway, C. E., & Muller, C. (2018). Convective self-aggregation in numerical simulations: A review. Shallow clouds, water vapor, circulation, and climate sensitivity (pp. 1–25).

Wood, R., & Bretherton, C. S. (2006). On the relationship between stratiform low cloud cover and lower-tropospheric stability. *Journal of Climate*, *19*(24), 6425–6432. https://doi.org/10.1175/jcli3988.1

Zhang, B., Soden, B. J., Vecchi, G. A., & Yang, W. (2021). Investigating the causes and impacts of convective aggregation in a high resolution atmospheric GCM. *Journal of Advances in Modeling Earth Systems*, *13*(11), e2021MS002675. https://doi.org/10.1029/2021ms002675

Zhang, B., Zhao, M., & Tan, Z. (2023). Using a Green's function approach to diagnose the pattern effect in GFDL AM4 and CM4. *Journal of Climate*, *36*(4), 1105–1124. https://doi.org/10.1175/jcli-d-22-0024.1

Zhang, Y., & Fueglistaler, S. (2019). Mechanism for increasing tropical rainfall unevenness with global warming. *Geophysical Research Letters*, *46*(24), 14836–14843. https://doi.org/10.1029/2019gl086058

Zhang, Y., & Fueglistaler, S. (2020). How tropical convection couples high moist static energy over land and ocean. *Geophysical Research Letters*, *47*(2), e2019GL086387. https://doi.org/10.1029/2019gl086387

Zhang, Y., Jeevanjee, N., & Fueglistaler, S. (2020). Linearity of outgoing longwave radiation: From an atmospheric column to global climate models. *Geophysical Research Letters*, *47*(17), e2020GL089235. https://doi.org/10.1029/2020gl089235

Zhao, M., Golaz, J.-C., Held, I., Guo, H., Balaji, V., Benson, R., et al. (2018a). The GFDL global atmosphere and land model AM4.0/LM4.0: 1. Simulation characteristics with prescribed SSTs. *Journal of Advances in Modeling Earth Systems*, *10*(3), 691–734. https://doi.org/10.1002/2017ms001208

Zhao, M., Golaz, J.-C., Held, I., Guo, H., Balaji, V., Benson, R., et al. (2018b). The GFDL global atmosphere and land model AM4.0/LM4.0: 2. Model description, sensitivity studies, and tuning strategies. *Journal of Advances in Modeling Earth Systems*, *10*(3), 735–769. https://doi.org/10.1002/2017ms001209

Zhou, C., Zelinka, M. D., & Klein, S. A. (2016). Impact of decadal cloud variations on the Earth's energy budget. *Nature Geoscience*, *9*(12), 871–874. https://doi.org/10.1038/ngeo2828

Zhou, C., Zelinka, M. D., & Klein, S. A. (2017). Analyzing the dependence of global cloud feedback on the spatial pattern of sea surface temperature change with a Green's function approach. *Journal of Advances in Modeling Earth Systems*, *9*(5), 2174–2189. https://doi.org/10.1002/2017ms001096